Outage Probability Analysis for Distributed Antenna System with Cooperative Transmission Schemes

Fei Xiong *†, Jianhua Zhang †, Ping Zhang †
* Wireless Technology Innovation Institute, †Key Laboratory of Universal Wireless Communication, Ministry of Education
Beijing University of Posts and Telecommunications, Beijing 100876, P. R. China
Email: xiongfei@mail.wtilabs.cn

***Abstract*—In this paper we utilize the cooperative transmission schemes in distributed antenna system (DAS). Since the distributed antennas are sufficiently separated with each other, therefore it is reasonable to assume the transmitted signals undergo independent fading channels with non-identical distribution. By using of the moment generation function, we deduced the numerical expression of outage probability from Gauss-Chebychev quadrature. Furthermore we conducted an extensive channel measurement, which verifies the advantage of cooperative transmission schemes under the composite fading conditions.**

I. INTRODUCTION

With the development of next generation mobile communications, distributed antenna system (DAS) has attracted wide research interests in recent years, because it provides an effective way to improve capacity and increase system throughput [1]–[3]. In [3] Saleh was the first to put forward the concept of distributed antennas to solve the coverage problem in the indoor radio communication systems. From the perspective of previous studies, DAS could also decrease the outage probability and enhance the signal quality dramatically [4]–[6]. According to simulation results, the authors in [4], [5] studied the outage performance of DAS, but it is not logical to assume all signals undergo identical fading channels in the real radio propagation conditions. In [6] the authors submitted the cooperative transmission schemes between geographically closed user terminals, however, without considering cooperation schemes between adjacent antenna ports.

Motivated by previous work, in this study we analyzed the downlink cellular DAS performance with composite fading conditions. By using of moment generation function, the numerical solution of outage probability is derived from Gauss-Chebychev quadrature. Furthermore we conducted an extensive channel measurement in the indoor environment to realize the considered model, where the experimental results validate the advantage of cooperative transmission schemes.

The remainder of this paper is organized as follows. Section II describes the system structures and fading channel model. Section III gives the analytical expression for the outage probability. Section IV and the Section V shows the simulation and experimental results independently including a discussion of those results. Finally the Section VI draws a brief conclusion of the subjects discussed in the previous sections.

CHINACOM 2010, August 25-27, Beijing, China

DOI 10.4108/iwoncmm.2010.4

II. SYSTEM DESCRIPTION AND CHANNEL MODEL

A. System Description

As well-known that the traditional centralized antenna system (CAS) is interference limited system, in which the base station (BS) is assumed located in the geometrical center within each cell. However, under such denotations BS cannot guarantee marginal signal qualities. Because the received signals would be affected by path loss, deep shadow fading and multipath delay. All of these factors will cause unreliable link quality and worse quality of service (QoS) standard. So we change our mind to make use of cooperative transmission schemes, where the identical signals transmit from k ($k \geq 2$) multiple AEs simultaneously. In such a way, we convert the interference signals of adjacent AEs into useful information, and make it possible to have higher marginal throughput, lower outage probability and reliable link quality.

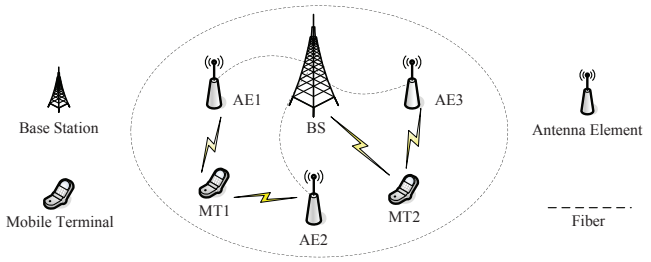

Fig. 1. The considered structure of distributed antenna system.

The considered DAS architecture can be illustrated from Fig. 1, where the antenna elements (AEs) geographically distributed in the hexagonal cells with common radius of R. All of the BSs and AEs are physically connected by coaxial cables or optical fibers between each other. Under such denotation we can utilize the cooperative transmission schemes, where the channel state information (CSI) could be shared partially or entirely between adjacent AEs. For example, when instantaneously channel conditions from the AE1 to mobile terminal (MT1) is not preferable, and then AE2 could participate in cooperative communication collectively. Different from previous study, here the central BS works not only as a controller but also as a scheduler, where the central base station coordinates the adjacent AEs to work together for the mobile users. In marginal areas, AEs are equipped with

power amplifier and low noise amplifier to fulfill the signal collection and amplification function, where we can process the enormously data effectively and make the computation burden of radio remote unit as low as possible.

Compared with the conventional DAS architecture, the total number of antennas in the considered cellular system has been reduced, therefore we can simplify the network architecture and decrease the number of co-channel interference simultaneously.

B. Channel Model

In the considered system we mainly concern about the downlink flat fading channel models which include path loss, lognormal shadowing and small-scale fading (Rician /Nakagami-m fading). Hence, the received signal at MT could be expressed as

$$y = \sqrt{P}hx + z \ , \tag{1}$$

where x represents transmit signals with $E[|x|^2] = 1$ [1] and $\sqrt{P}$ is signal power from kth AE to MT, symbol z is complex additive white Gaussian noise (AWGN) with variance σ_z^2, the channel vector h can be expressed as

$$h = (h^{(1)}, h^{(2)}, ..., h^{(k)}, ..., h^{(N)})^T, \tag{2}$$

where $(.)^T$ denotes the transpose operator, the upper note k of $h^{(k)}$ stands for the signal transmit from k th AE ($k = 1, 2 \ldots, N$) to MT. In order to make it clear, we can rewrite $h^{(k)}$ as

$$h^{(k)} = s^{(k)} \sqrt{l^{(k)}} \ . \tag{3}$$

In this study we use two different models to describe small scale parameter $s^{(k)}$ when considering the practical radio propagation environments. Here Rician distribution and Nakagami-m distribution are selected to model desired signals and interference signals respectively, where Rician fading channel describe the line of sight condition and Nakagami-m depict more severe fading channel conditions.

The second term $l^{(k)}$ is modeled as log-normal distributed random variable and its probability density function (PDF) is denoted by

$$f_{l^k}(\psi) = \frac{\varepsilon}{\sqrt{2\pi}\sigma^{(k)}\psi} \exp(-\frac{(10\log_{10}\psi - \mu^{(k)})^2}{2(\sigma^{(k)})^2}) \ , \tag{4}$$

where $\varepsilon = \frac{10}{\ln 10}$, ψ is the power ratio between transmitted signals and received signals, $\mu^{(k)}$ (in dB) is the mean of $10\log_{10}\psi$, and $\sigma^{(k)}$ (in dB) is standard deviation of $10\log_{10}\psi$. In this paper we use $\mathcal{A}$ and $\mathcal{B}$ denote the sets of desired signals and interference signals separately, and then (1) can be rewritten as

$$y = \sum_{i\in\mathcal{A}} \sqrt{P}h^{(i)}x^{(i)} + \sum_{j\in\mathcal{B}} \sqrt{P}h^{(j)}x^{(j)} + z \ , \tag{5}$$

where we define $Y^{(i)} = P\left\|h^{(i)}\right\|^2\left\|x^{(i)}\right\|^2$ ($i \in \mathcal{A}$) and $Y^{(j)} = P\left\|h^{(j)}\right\|^2\left\|x^{(j)}\right\|^2$ ($j \in \mathcal{B}$) as the power of the desired signals and interference separately, and $\|\cdot\|$ is the Euclidean-norm. Here, the PDF of $Y^{(i)}$ is in accordance with Lognormal-Rician distribution which can be expressed as

$$\begin{aligned} f_{Y^{(i)}}(y) \quad = \quad & \int_0^\infty \frac{\varepsilon}{\sqrt{2\pi}\sigma^{(i)}\psi^{(i)}} \exp\left[\frac{-(10\log_{10}\psi - \mu^{(i)})^2}{2(\sigma^{(i)})^2}\right] \\ & \cdot \frac{(1+K^{(i)})}{\psi^{(i)}} \exp(-K^{(i)} - \frac{1+K^{(i)}y}{\psi^{(i)}}) \\ & \cdot I_0\left[2\sqrt{\frac{K^{(i)}(K^{(i)}+1)y}{\psi^{(i)}}}\right] d\psi^{(i)} \ . \end{aligned} \tag{6}$$

Similarly the PDF of $Y^{(j)}$ is in accordance with Lognormal-Nakagami-m distribution, which is given by

$$\begin{aligned} f_{Y^{(j)}}(y) \quad = \quad & \int_0^\infty \frac{\varepsilon}{\sqrt{2\pi}\sigma^{(j)}\psi^{(j)}} \exp\left[\frac{-(10\log_{10}\psi - \mu^{(j)})^2}{2(\sigma^{(j)})^2}\right] \\ & \cdot \frac{y^{m^{(j)}-1}(m^{(j)})^{m^{(j)}}}{(\psi^{(j)})^{m^{(j)}}\Gamma(m^{(j)})} \exp(\frac{-m^{(j)}y}{\psi^{(j)}}) d\psi^{(j)} \ , \end{aligned} \tag{7}$$

where the symbol K in (6) represents Rician K factor and symbol m in (7) is the Nakagami-m fading parameter with the ranges from 1/2 to infinite. Under such assumption, the instantaneous signal-to-interference ration (SIR) is

$$\gamma = \sum_{i=1}^{U} Y^{(i)} \Big/ \sum_{j=1}^{V} Y^{(j)} \ , \tag{8}$$

where the effect of background noise is negligible when compare with interference signals, and U, V is the number of desired signals and interference signals respectively.

III. NUMERICAL ANALYSIS

A. Approximation for Outage Probability

In this study we define P_{out} as the probability that the instantaneous error probability exceeds a specified value which the output SIR, γ , falls under a certain threshold, γ_{th} ,mathematically speaking ,we have

$$P_{out} = F(\gamma) = p(\gamma < \gamma_{th}) = \int_0^{\gamma_{th}} f(\gamma)d\gamma \ , \tag{9}$$

where $F(\gamma)$ is the cumulative distribution function (CDF) of γ, p is probability function, and $f(\gamma)$ denotes the PDF of γ. By using of Laplace transform we deduce the relationship between $F(s)$ and $f(s)$ by

$$F(s) = f(s)/s \ . \tag{10}$$

As can be seen from (8) the distribution of γ is hard to be written in close form. Then we try to utilize the property of moment generation function (MGF) to give an analytical solution. The expression of MGF can be written as

$$\varphi(s) = \int_0^\infty f(\gamma)\mathrm{e}^{s\gamma}d\gamma \ . \tag{11}$$

According to the Laplace transform, $\varphi(s)$ and $f(s)$ are related by $f(s) = \varphi(-s)$. We substitute it into equation (10),

[1] $E[.]$ is expectation operator

and then the outage probability can be derived from inverse Laplace transform as

$$P_{out} = \frac{1}{2\pi j}\int_{\sigma-\infty}^{\sigma+\infty}\frac{\varphi(-s)}{s}e^{s\gamma_{th}}ds\ , \tag{12}$$

where s is replaced by $\lambda + j\omega$ ($\lambda < 0$), hence, the integrand function $\varphi(-s)/s$ has left plane pole to keep integral convergent into finite boundary. For the sake of simplicity the threshold γ_{th} has been set to 0 (dB), then we can get the following expression

$$\begin{aligned} P_{out} &= \frac{1}{2\pi}\int_{-\infty}^{+\infty}\frac{\varphi(-(\lambda+j\omega))}{\lambda+j\omega}d\omega \\ &= \frac{1}{\pi}\int_{0}^{+\infty}\frac{\mathrm{Re}al\{(\lambda+j\omega)\varphi(-(\lambda+j\omega)\}}{\lambda^2+\omega^2}d\omega\ . \end{aligned} \tag{13}$$

In order to obtain the numerical expression, we utilize the methods introduced by Annamalai [7], [8], where the integral expression can be approximated by a Gauss-Chebychev quadrature and symbol ω can be substituted by $a\tan(\phi/2)$. Then we derive the expression as

$$P_{out} = \frac{1}{2I}\sum_{i=1}^{I}\eta((\frac{i}{I}-\frac{1}{2I})\pi)\ , \tag{14}$$

where I is the iteration number and we set $I = 10$ when considering the calculation speed and the system tolerance (error rate $\varepsilon \le 10^{-3}$), and the integrand function $\eta(.)$ in (14) can be denoted by

$$\eta(\phi) = \mathrm{Re}al\{(1-j\tan(\phi/2))\varphi(-\lambda(1+j\tan(\phi/2)))\}\ . \tag{15}$$

B. Numerical Formula by using MGF

Here we try to obtain the MGF expression of Lognormal-Rician and Lognormal Nakagami-m distribution separately, and in the aid of Laplace transform and Hermite integration [9], we can convert (6) into (16)

$$\begin{aligned} \varphi_D(s) &= \frac{1}{\sqrt{\pi}}\sum_{l=1}^{L}\frac{\xi_l(1+K^{(i)})}{1+K^{(i)}-s\mu^{(i)}e^{\sqrt{2}\sigma^{(i)}x_l}} \\ &\quad .\ \exp(\frac{sK^{(i)}\mu^{(i)}e^{\sqrt{2}\sigma^{(i)}x_l}}{1+K^{(i)}-s\mu^{(i)}e^{\sqrt{2}\sigma^{(i)}x_l}})\ , \end{aligned} \tag{16}$$

where $\varphi_D(s)$ stands for the MGF of desired signals, $\mu^{(i)}$ and $\sigma^{(i)}$ are local mean power and standard deviation separately, the coefficients ξ_l and x_l are the weight factors of the l-order Hermite polynomial and lth root respectively. Similarly the PDF of interference signals with (7) can be expressed as

$$\varphi_I(s) = \frac{1}{\sqrt{\pi}}\sum_{l=1}^{L}\xi_l(1-s\mu^{(j)}e^{\sqrt{2}\sigma^{(j)}x_l}\Big/m^{(j)})^{-m^{(j)}}\ , \tag{17}$$

where $\varphi_I(s)$ is the MGF of interference signal, $m^{(j)}$ is fading severity index, symbol ξ_l, $\mu^{(j)}$ and $\sigma^{(j)}$ have the same meaning with that in (16). Then the MGF of SIR can be given by

$$\varphi_\gamma(s) = \prod_{i=1}^{U}\varphi_{D,i}(s)\prod_{j=1}^{V}\varphi_{I,j}(-s)\ . \tag{18}$$

Combine (14) with (18), we can derive the final numerical outage expression as

$$\begin{aligned} P_{out} &= \frac{1}{2I}\sum_{j=1}^{I}\mathrm{Re}al\{(1-j\tan((\frac{i}{I}-\frac{1}{2I})\pi/2))\} \\ &\quad .\ \{\varphi_\gamma(-\lambda(1+j\tan((\frac{i}{I}-\frac{1}{2I})\pi/2)))\}\ . \end{aligned} \tag{19}$$

IV. NUMERICAL EVALUATION AND DISCUSSION

In this part we try to evaluate the performance of considered DAS architecture in Section II. The simulation parameters are list as following, where the Nakagami-m fading severity index m is arranged in descendent order according to the distance from AEs to MT, and the smaller index m corresponds to more severe fading condition with longer distance. While several other parameters such as local mean power $\mu^{(k)}$, standard deviation $\sigma^{(k)}$ and K factors are recommended by ITU-R under indoor hotspot (InH) scenario [10], and the total transmit power in each cell is limited to $\mathcal{P}$. Under such denotation, we randomly place the positions of mobile user with a common radius of R=100m under InH scenario. For the sake of fairness, we keep the amount of positions in direct proportion with the area of given cell, e.g., $N_p \propto \lambda\pi R^2$, where N_p is the number of randomly generated position, and $\lambda = 0.5$ is the tradeoff between computation speed and precision.

By using of (19) we obtain the outage probability as shown in Fig. 2. Here we first simulate the outage performance of traditional hexagonal centralized antenna systems. The interference signals come from the six co-channel BSs in adjacent cells and no channel state information be shared between each cells. From the simulation results we can find that the central area has better signal quality with significantly lower outage probability, however, in the marginal area the system performance become worse when user moves far away from BS.

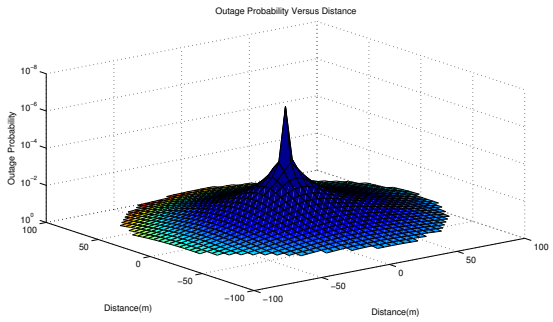

Fig. 2. The outage probability of traditional centralized antenna system with six co-channel interference signals.

The non-cooperative transmission has been shown in Fig. 3, where each time MT communicates with the nearest AE according to the instantaneous channel conditions. As can be seen from Fig. 3, when MT randomly located in the DAS cells, the outage performance has not fluctuated wildly between central areas and borders, furthermore, the quality of received

signals in marginal areas has considerable improvement when compared with traditional centralized antenna systems.

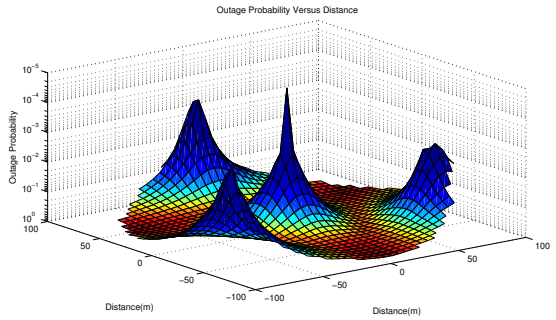

Fig. 3. The outage probability of distributed antenna system with non-cooperative transmission schemes.

The results of cooperative transmission schemes have been shown in Fig. 4, where several adjacent AEs transmit the identical signals to MT simultaneously. Here we denote BS as a central AE, and then up to four adjacent AEs could participate into cooperative transmission together. According to the simulation results in Fig.4, the cooperative transmission schemes are depicted with dash-dotted vertical ellipse, where it performs much better than non-cooperative transmission with the increase of the participated antennas numbers. Furthermore, according to the ordinate value in Fig.3, the gap has gradually enlarged at the given the SIR value, e.g., SIR equal to 20 dB. Therefore under the composite fading conditions cooperative transmission schemes have shown more attractive property than that with non-cooperative transmission schemes, and this could provide the guideline for the application of the distributed mobile communications.

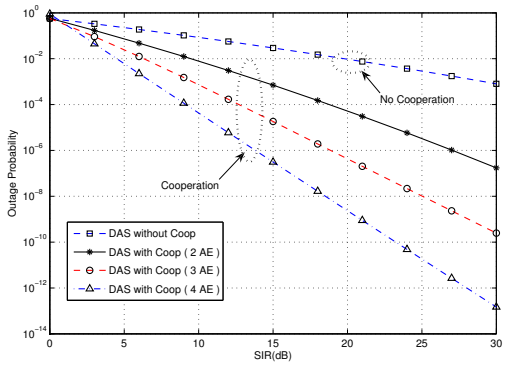

Fig. 4. The comparison between cooperative and non-cooperative transmission schemes under composite fading conditions.

V. EXPERIMENTAL COMPARISION AND DISCUSSION

In Section IV we simulate the performance of cooperative transmission schemes under the considered cellular structure. Here we try to testify the system performance through practical experiments as shown in the following part.

A. Equipments and Scenarios

Extensive channel measurements were performed at the Beijing University of Posts and Telecommunications (BUPT), Beijing, China. Measured channel data were recorded by utilizing Elektrobit Propsound Channel Sounder, which used periodic pseudorandom binary signals of 511 sequence length and time-division mode. The center frequency was 4.9 GHz with a chip rate of 100 MHz. As can be seen from Fig.5 that the receiver employed a vertical-polarized dipole and the transmitter mounted two vertical-polarized dipoles. (To make it clear, here we denote receiver as MT and transmitter as AE). Furthermore the two separated AEs were located at the entrance of corridor and in the center of the hall independently, namely AE-1 and AE-2 separately.

As shown in Fig. 5, the measurements were carried out in the ground floor of a teaching building with the dimension of a single floor about 120 m $\times$ 45 m $\times$ 6 m, while the transmit power at antenna input was set to 23 dBm in all cases. During the measurements MT moved along the planed routes denoted as circles with antenna height of about 1.5 m and AEs were kept fixed all the time with antennas height of about 2.5 m. For each stationary measurement location, 500 snapshots of channel responses were recorded for post processing.

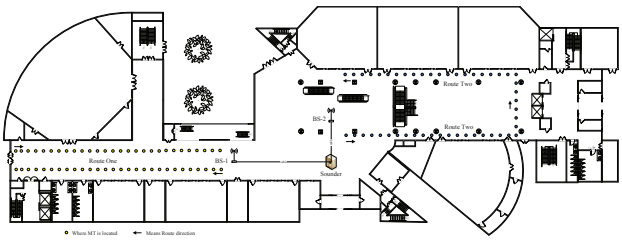

Fig. 5. Architectural plans of indoor measurement scenarios.

B. Measurement Analysis and Discussion

In this part we conducted a series of analysis based on the raw data collected in Section V. The measured data combined the effect of system impulse response and channel impulse response (CIR). In order to accurately describe the propagation characteristic, measured data were cyclically correlated with spread signals known as PN codes to obtain the CIR, thus the effect of system impulse response can be removed from sounding system. According to the measured results, we can obtain the local power delay profile (PDP) by averaging the received power for each snapshot of channel response. After that, linear regression in a minimum mean square error (MMSE) sense is utilized to derive the path loss and shadow fading separately. Here the outage probability $P_{out}(d)$ under path loss and shadowing is defined as the received power at a given distance, d , falls below target minimum received power level $P_{\min}$ (Referred to [11] in Section 2.9).

Under such denotation, we will compare two different radio propagation conditions (Racian/Nakagami-m fading) with several separated AEs. To begin with, we assume the non-cooperative transmission case that the received signals come

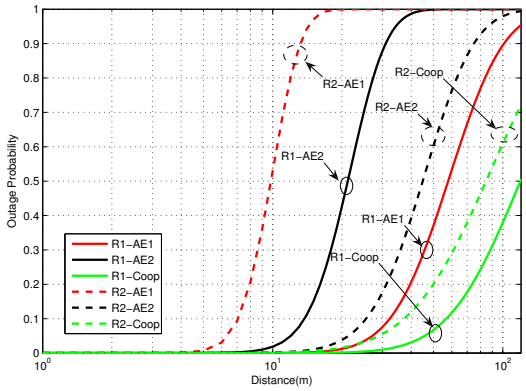

Fig. 6. The channel measurement with cooperative and non-cooperative transmission schemes under composite fading conditions.

from AE-1. In this case, when MT moved along route one (R1), the Rician components hold the leading place (Represent by R1-AE1 in Fig. 6). However when measurement was employed along route two (R2), the Nakagami-m components take the important role (Denote as R2-AE1 in Fig. 6). As shown in Fig. 6, we can observe that the outage performance of R1-AE1 (Rician fading) is better than that with R2-AE1 (Nakagami-m fading) at the same distance. While the opposite is true when it comes to AE2, in which R1-AE2 is inferior to R2-AE2. This implies that the single port transmission of GDAS cannot be well implemented under sever fading conditions (Nakagami-m fading).

However, in Fig. 6 the rightmost two curves have shown the performance of cooperative transmission schemes that the data stream transmit from AE1 and AE2 simultaneously with CSI shared between each other. According to the simulation results, in all cases (R1/R2) the cooperative transmit schemes have shown more favorable performance with lower outage probability and longer access distance when compared with the left four curves. Based on the results we can draw a conclusion reasonably that the separated antenna with single port transmission cannot exert the full potential of distributed antennas, whereas, the cooperative transmit schemes can improve the performance remarkably under the composite fading conditions.

VI. CONCLUTIONS

In this paper, we have studied cooperative transmission schemes under GDAS architectures. Due to the geographical separated antenna elements with longer distance between each other, we assume the transmitted signals undergo independent and non-identical fading. Under such assumption numerical expression of outage probability has been deduced from Gauss-Chebychev quadrature. Furthermore extensive channel measurements were employed under composite fading conditions, in which the cooperative transmission schemes have shown much more attractive properties with much lower outage probability and longer access distance when compared with single port transmission schemes.

VII. ACKNOWLEDGMENT

The research is funded by China 863 Program under Grant NO. 2009AA011502 and China Important National Science & Technology Specific Projects under Grant NO.2009ZX03007-003-01 and by National Natural Science Foundation of China under Grant NO. 60772113.

REFERENCES

[1] W. Roh and A. Paulraj, "MIMO channel capacity for the distributed antenna," in *Proc. VTC 2002-Fall Vehicular Technology Conference 2002 IEEE 56th*, vol. 2, 24–28 Sept. 2002, pp. 706–709.

[2] A. Paulraj and W. Roh, "Performance of the distributed antenna systems in a multi-cell environment," in *Proc. VTC 2003-Spring Vehicular Technology Conference The 57th IEEE Semiannual*, vol. 1, 2003, pp. 587–591 vol.1.

[3] A. Saleh, A. Rustako, and R. Roman, "Distributed antennas for indoor radio communications," *IEEE Trans. Commun.*, vol. 35, no. 12, pp. 1245–1251, Dec 1987.

[4] F. Berggren and S. B. Slimane, "A simple bound on the outage probability with lognormally distributed interferers," *IEEE Commun. Lett.*, vol. 8, no. 5, pp. 271–273, May 2004.

[5] Y. Zhao, R. Adve, and T. J. Lim, "Outage probability at arbitrary snr with cooperative diversity," *IEEE Commun. Lett.*, vol. 9, no. 8, pp. 700–702, 2005.

[6] Y. Chen, L. Hu, C. Yuen, Y. Zhang, Z. Zhang, and P. Rapajic, "Intrinsic measure of diversity gains in generalised distributed antenna systems with cooperative users," *IET Communications*, vol. 3, no. 2, pp. 209–222, 2009.

[7] C. Tellambura and A. Annamalai, "An unified numerical approach for computing the outage probability for mobile radio systems," *IEEE Commun. Lett.*, vol. 3, no. 4, pp. 97–99, April 1999.

[8] A. Annamalai, C. Tellambura, and V. K. Bhargava, "Simple and accurate methods for outage analysis in cellular mobile radio systems-a unified approach," *IEEE Trans. Commun.*, vol. 49, no. 2, pp. 303–316, Feb 2001.

[9] D. Z. Alan Jeffrey, *Table of Integrals, Series, and Products, Seventh Edition*, D. Z. Alan Jeffrey, Ed. Academic Press, 2007-02-23.

[10] ITU-R WP5D, "Guidelines for evaluation of radio interface technologies for IMT-Advanced," Document 5D/TEMP/99-E, Oct. 2008.

[11] A. Goldsmith, *Wireless Communications*. Cambridge University Press, 2005.